JACS
JOURNAL OF THE AMERICAN CHEMICAL SOCIETY

Article

pubs.acs.org/JACS

Crystallization in Sequence-Defined Peptoid Diblock Copolymers Induced by Microphase Separation

Jing Sun,[†,‡] Alexander A. Teran,[⊥,§] Xunxun Liao,[#,∥] Nitash P. Balsara,*[,⊥,‡,§] and Ronald N. Zuckermann*[,†,‡]

[†]Molecular Foundry, [‡]Materials Sciences Division, [§]Environmental Energy Technologies Division, and [∥]National Center for Electron Microscopy, Lawrence Berkeley National Laboratory, Berkeley, California 94720, United States

[⊥]Department of Chemical and Biomolecular Engineering and [#]Department of Materials Science and Engineering, University of California, Berkeley, California 94720, United States

Supporting Information

ABSTRACT: Atomic level synthetic control over a polymer's chemical structure can reveal new insights into the crystallization kinetics of block copolymers. Here, we explore the impact of side chain structure on crystallization behavior, by designing a series of sequence-defined, highly monodisperse peptoid diblock copolymers poly-*N*-decylglycine-*block*-poly-*N*-2-(2-(2-methoxyethoxy)ethoxy)-ethylglycine (pNdc-*b*-pNte) with volume fraction of pNte (ϕ_{Nte}) values ranging from 0.29 to 0.71 and polydispersity indices ≤1.00017. Both monomers have nearly identical molecular volumes, but the pNte block is amorphous while the pNdc block is crystalline. We demonstrate by X-ray scattering and calorimetry that all the block copolypeptoids self-assemble into lamellar microphases and that the self-assembly is driven by crystallization of the pNdc block. Interestingly, the microphase separated pNdc-*b*-pNte diblock copolymers form two distinct crystalline phases. Crystallization of the normally amorphous pNte chains is induced by the preorganization of the crystalline pNdc chains. We hypothesize that this is due to the similarity of chemical structure of the monomers (both monomers have linear side chains of similar lengths emanating from a polyglycine backbone). The pNte block remains amorphous when the pNdc block is replaced by another crystalline block, poly-*N*-isoamylglycine, suggesting that a close matching of the lattice spacings is required for induced crystallization. To our knowledge, there are no previous reports of crystallization of a polymer chain induced by microphase separation. These investigations show that polypeptoids provide a unique platform for examining the effect of intertwined roles of side chain organization on the thermodynamic properties of diblock copolymers.

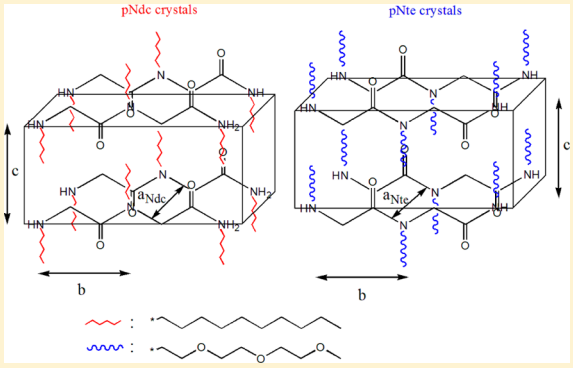

INTRODUCTION

Research on polymer crystallization is driven by both fundamental and practical considerations. A large fraction of commercially important polymers such as polyethylene and polypropylene are crystalline. Polymer molecules participating in crystallization adopt folded conformations that are fundamentally different from those found in conventional crystals formed by small molecules.[1−7] There is thus a great interest in the mechanism by which nucleation barriers are overcome during polymer crystallization. In this paper, we study microphase separation in diblock copolymers wherein one of the blocks is inherently crystalline while the other is inherently amorphous. By inherently amorphous, we mean that homopolymers with the same segment could not be crystallized, regardless of molecular weight and thermal history. We demonstrate that self-assembly of the copolymer chains into lamellar phases induces crystallization of the inherently amorphous block. To our knowledge, there are no previous reports suggesting that nucleation barriers to polymer crystallization of one block can be overcome by preorganization of the other block of a crystalline block copolymer.

In the case of block copolymers with one or more crystallizable blocks, it is important to distinguish between crystalline order reflecting the periodic order on the atomic length scale and order formation due to microphase separation reflecting the periodic arrangement of domains on molecular length scales. The packing of chain folded lamellar crystals inside lamellar microphases has been discussed extensively in previous publications.[8−16] Much of the work on crystalline block copolymers is on systems where one of the blocks is crystalline and the other is amorphous. The microphase separated morphology of these systems depends mainly on the segregation strength between the blocks and free energy of crystallization. The segregation strength is governed by the product χN, where χ is the Flory−Huggins interaction parameter and N is the number of segments per chain. When

Received: November 27, 2013
Published: January 15, 2014

   dx.doi.org/10.1021/ja412123y | *J. Am. Chem. Soc.* 2014, 136, 2070−2077

Table 1. Block/Homo Polypeptoid pNdc$_n$-*b*-pNte$_m$ Synthesized and Their Characteristics[d]

pNdc$_n$-*b*-pNte$_m$	m	n	ϕ_{Nte}	Molar mass (calc/obs)	Purity(%)[a]	PDI[c]
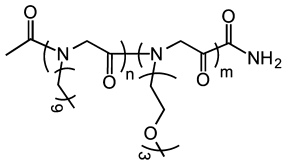	10	0	1	2091.2/2090.4	90	1.00077
	27	0	1	5546.2/5553.8	80	1.00019
	27	9	0.71	7320.8/7319.6	83	1.00014
	21	12	0.59	6693.6/6684.7	75	1.00013
	18	18	0.45	7267.3/7263.1	90	1.00011
	12	24	0.29	7232.7/7233.5	80[b]	1.00017
	0	10	0	2031.8/2036.8	90	1.00049
	0	15	0	3018.7/3023.8	90[b]	1.00042
	0	20	0	4004.6/4010.5	70[b]	1.00090
pNia$_n$-*b*-pNte$_m$	18	18	-	6004.9/6009.7	95	1.00003

[a]Purity is the weight fraction of full-length polymer as determined by analytical HPLC. The remaining impurities are primarily full-length polymers missing one or two residues. [b]As estimated by MALDI. [c]PDI = polydispersity, is calculated based on the HPLC and MALDI data as in ref 36. [d]Molar mass was determined by MALDI mass spectrometry.

χN is very small, microphase separation is driven by the free energy of crystallization.[17] In this case, lamellar microphases are obtained regardless of the compositions of the polymers, due to the fact that chain folding results in lamellar crystals. As χN increases, the resulting morphology depends on the competition between the two thermodynamic driving forces.[11,18−20] In the weak segregation limit (small χN), the crystals "breakout" of the block copolymer microphase.[11,20] In the strong segregation limit (large χN), crystalline order is confined within conventional block copolymer microphases such as lamellae, cylinders, and spheres.[8,19]

Some studies have been conducted on block copolymers wherein both blocks are crystallizable.[14,21−24] Lin et al. studied crystallization of syndiotactic polypropylene-*b*-poly(ε-caprolactone) (sPP-*b*-PCL). They showed that crystallization of the PCL block was accelerated by the presence of crystalline sPP.[22] Ding et al. studied crystallization of a low molecular weight polyethylene-*b*-poly(ethylene oxide)-*b*-polyethylene (PE-PEO-PE) sample.[23] PEO homopolymer chains exhibit a helical conformation in the crystals, while PEO blocks in PE-*b*-PEO-*b*-PE exhibit a zigzag conformation. In both of these studies,[22,23] the unexpected crystallization behaviors of PCL and PEO were ascribed to chain stretching induced by microphase separation. Li et al. conducted simulations on diblock copolymers with two crystallizable blocks.[24] They showed that crystallization of the block with the lower melting temperature was accelerated by the presence of crystals of the higher melting block. However, none of these studies address the possibility of forming two crystalline phases in diblock copolymers comprising crystalline and amorphous chains. Importantly, all the crystalline polymer samples described above are semicrystalline in that they contain coexisting crystalline and amorphous regions.

In order to probe the effect of monomer structure on polymer crystallization and microphase separation more precisely, we designed a set of sequence-specific polypeptoid block copolymers. Polypeptoids are a family of comblike polymers based on an N-substituted glycine backbone.[25−30] They offer tremendous advantages for material science in the solid state. The lack of hydrogen-bond donors along the main chain (as compared to peptides and many other peptidomimetic polymers) results in a flexible backbone with reduced interchain interactions and excellent thermal processability.[31]

The solid-phase submonomer synthesis method allows for the efficient synthesis of polymers with precise control over the monomer sequence and side chain structure, since the side chains are introduced from an extremely diverse set of primary amine building blocks.[26,32] Previous work by Rosales et al. explored the relationship between the molecular structure and crystallization behavior of homopolypeptoids.[33] They also studied the effect of introducing monomeric defects on crystallization and melting. In the present research, we designed and synthesized a series of poly-*N*-decylglycine-*block*-poly-*N*-2-(2-(2-methoxyethoxy)ethoxy)ethylglycine (pNdc-*b*-pNte) with volume fraction of pNte (ϕ_{Nte}) values ranging from 0.29 to 0.71. The polydisperisty indices of all the pNdc-*b*-pNte copolymers is 1.00017 or less. Superficially, this block copolypeptoid has one crystalline pNdc block and one amorphous pNte block;[34,35] in spite of imposing several thermal histories, we were unable to crystallize pNte homopolymers. We previously studied the microphase separation of the amorphous diblock copolypeptoids poly-*N*-(2-ethyl)hexylglycine-*block*-poly-*N*-2-(2-(2-methoxyethoxy)-ethoxy)ethylglycine (pNeh-*b*-pNte),[36] which exhibits lamellar morphology with ϕ_{Nte} ranging from of 0.11 to 0.49. Unlike our previous study, all the crystalline block copolypeptoids in this study self-assemble into lamellar structures driven by crystallization of the pNdc block. It was observed that both pNte and pNdc lamellae are crystalline at low temperatures. We argue that the crystalline nature of the pNdc block induces crystallization of the pNte block. In other words, precrystallization of the pNdc block and the resulting microphase separation enables overcoming nucleation barriers that prevent crystallization of pNte homopolymer chains. Furthermore, the pNte block remains amorphous when the pNdc block is replaced by another crystalline block, poly-*N*-isoamylglycine (pNia). We posit that the ability of the pNdc block to induce crystallization of the pNte block is due to the similarity of chemical structure of the monomers and their resultant lattice structures in the crystal (both monomers have linear side chains containing 10 non-hydrogen atoms, emanating from a polyglycine backbone).

RESULTS AND DISCUSSION

A series of sequence-defined $pNdc_n$-*b*-$pNte_m$ copolymers were synthesized by solid-phase synthesis and purified by HPLC, where the number of Nte monomers in the block copolymer is m, and the number of Ndc monomers is n (Table 1). Nearly all the samples have a fixed chain length ($m + n = 36$) and systematically vary the composition of the two blocks. We also studied the properties of pNte and pNdc homopolymers as indicated in Table 1. The phase behavior of these pNdc-*b*-pNte polymers was then investigated by small-angle X-ray scattering (SAXS), wide-angle X-ray scattering (WAXS), and differential scanning calorimetry (DSC).

We first investigated the morphology of pNdc-*b*-pNte copolymers by SAXS. In a typical SAXS profile of $pNdc_{12}$-*b*-$pNte_{21}$ at 25 °C, we see a primary peak at $q^* = 0.64$ nm^{-1} and higher-order peaks at $2q^*$ and $3q^*$, indicating the presence of a lamellar morphology (Figure 1). The prominent peak in the vicinity of $q = 2.5$ nm^{-1} is related to the side chain packing, and we will discuss this later in our discussion of wide-angle X scattering data. Increasing the temperature to 120 °C has virtually no effect on morphology (Figure 1a). Further increase of the sample temperature to 130 °C results in a dramatic decrease in the primary peak intensity and the primary peak splits in two. At 140 °C, a single broad peak with $q^* = 0.75$ nm^{-1} is obtained and scattering from the crystalline structure seen at $q = 2.5$ nm^{-1} disappears completely. The broadening of the primary peak is a standard signature of a lamellar-to-disorder transition in block copolymers.[37−39] As is the case with conventional block copolymers, this transition is reversible, as shown by the cooling data in Figure 1a. Cooling $pNdc_{12}$-*b*-$pNte_{21}$ to 125 °C results the reappearance of the peak $q = 2.5$ nm^{-1}, while the primary SAXS peak remains broad. Further cooling of the sample to 110 °C results in a SAXS profile that is identical to that obtained from the lamellar phase obtained during the heating run.

It is clear from Figure 1a that there is a significant change in q^* as $pNdc_{12}$-*b*-$pNte_{21}$ undergoes the lamellar-to-disorder transition. This is quantified in Figure 1b, where we plot q^* versus temperature for $pNdc_{12}$-*b*-$pNte_{21}$. At low temperatures, where the lamellar microphase is obtained, q^* is about 0.64 nm^{-1}, while at high temperatures, where the disordered phase is obtained, q^* is about 0.75 nm^{-1}. It is clear that at 130 °C during the heating run $pNdc_{12}$-*b*-$pNte_{21}$ contains coexisting ordered and disordered phases, as evidenced by the presence of a "doublet" in the SAXS profile; the locations of two maxima agree quantitatively with q^* obtained in the lamellar and fully disordered states. It is clear from Figure 1a,b that, unlike conventional block copolymers, the lamellar-to-disorder transition in $pNdc_{12}$-*b*-$pNte_{21}$ occurs in two steps. Between the lamellar (L) and disordered (D) phases is a metastable (M) window where nucleation barriers appear to be significant. The ranges of temperatures where these phases are obtained are shown in Figure 1b. The behavior in the metastable window is complex. SAXS profiles at 130 °C during the heating run and 125 °C during the cooling run show small but measurable peaks at $q = 2.5$ nm^{-1}, indicating the presence of crystals. However, broad primary SAXS peaks confirm the presence of disorder. Coexistence of phases in a one-component system cannot occur at equilibrium, as this would violate the Gibbs phase rule. Our observation of two-phase coexistence can, in principle, arise due to two reasons: (1) kinetic limitations due to small driving forces for the phase transition due to proximity

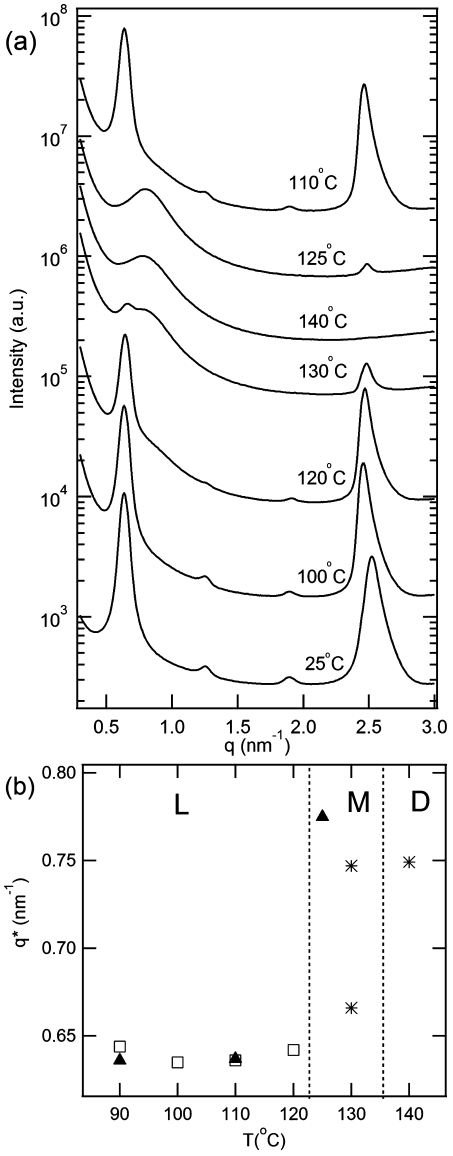

Figure 1. (a) SAXS intensity versus scattering vector, q, for $pNdc_{12}$-*b*-$pNte_{21}$. Profiles are vertically offset for clarity. (b) A plot of q^* of the primary peak versus temperature for $pNdc_{12}$-*b*-$pNte_{21}$, where L is the lamellar phase, D is the disordered phase, and M is the metastable window. Black open squares and stars plot the heating run and filled triangles plot the cooling run.

to the phase boundary, the reason why hysteresis is usually observed in the vicinity of melting transitions, or (2) the fact that our samples are strictly not one-component systems due to finite polydispersity (Table 1). Since the first reason is most likely to be correct, the thermodynamic lamellar-to-disorder transition is likely to be located somewhere in the metastable window.

The SAXS experiments described above were repeated for all the block copolymers listed in Table 1. All of them exhibited lamellar, metastable, and disordered windows. The locations of the windows, however, were different, as summarized in Table 2.

The thermal properties of homopolypeptoids and block copolypeptoids were investigated by DSC. As shown in Figure 2, the $pNdc_{20}$ homopolypeptoid melts over a narrow temperature range with a peak at 145 °C ($T_{m,Ndc}$) and an

dx.doi.org/10.1021/ja412123y | J. Am. Chem. Soc. 2014, 136, 2070−2077

Table 2. Transition Temperatures of the Block Copolypeptoids pNdc-*b*-pNte Obtained by SAXS ($T_{L\text{-}M}$ and $T_{M\text{-}D}$), DSC ($T_{m,Ndc}$ and $T_{m,Nte}$), and WAXS ($T_{wm,Ndc}$ and $T_{wm,Nte}$ = $T_{L''\text{-}L}$)

polymers	ϕ_{Nte}	$T_{L''\text{-}L}$(°C)	$T_{L\text{-}M}$(°C)	$T_{M\text{-}D}$(°C)	$T_{m,Ndc}$(°C)	$T_{m,Nte}$(°C)	$T_{wm,Ndc}$(°C)	$T_{wm,Nte}$(°C)
$pNdc_9$-*b*-$pNte_{27}$	0.71	45	95	105	91	44	95	45
$pNdc_{12}$-*b*-$pNte_{21}$	0.59	65	123	135	123	62	135	65
$pNdc_{18}$-*b*-$pNte_{18}$	0.45	65	135	148	138	66	145	65
$pNdc_{24}$-*b*-$pNte_{12}$	0.29	65	145	155	143	66	145	65

L″−L signifies the transition from lamellar phase with two crystalline blocks to lamellar phase with crystalline pNdc block; L−M signifies the transition from lamellar to metastable; M−D signifies the transition from metastable to disordered. $T_{m,Ndc}$ is the melting point of pNdc, and $T_{m,Nte}$ is the melting point of pNte by DSC. $T_{wm,Ndc}$ is the melting point of pNdc, and $T_{wm,Nte}$ is the melting point of pNte by WAXS.

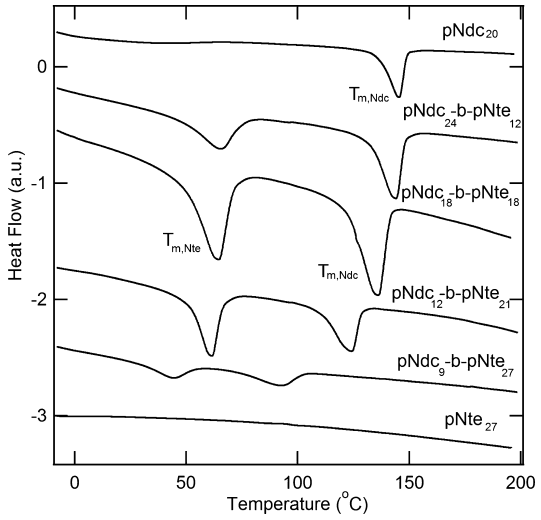

Figure 2. DSC endotherm of homopolypeptoids $pNte_{27}$, $pNdc_{20}$, and block copolypeptoids.

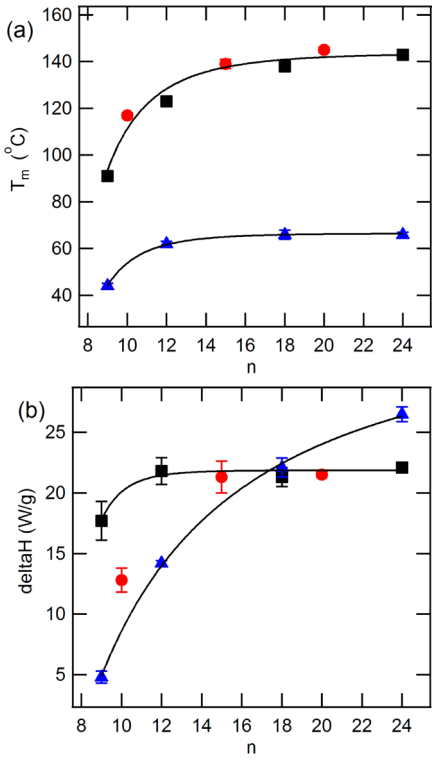

Figure 3. (a) Plots of T_m of pNdc and pNte in block copolypeptoids and homopeptoids by DSC versus *n* (chain length of pNdc block). (b) Plots of ΔH of pNdc and pNte in block copolypeptoids and homopeptoids by DSC versus *n* (chain length of pNdc block). In both panels, red circles plot pNdc homopolypeptoids, blue triangles plot pNte blocks, and black squares plot pNdc blocks in block copolypeptoids.

enthalpic change ($\Delta H_{m,Ndc}$) of 21 J/g. This result is consistent with previous results on a series of homopolypeptoids with short alkyl side chains.[33] The DSC data obtained from the $pNte_{27}$ homopolypeptoid were devoid of melting peaks, indicating a lack of crystalline order. The heating scan from this sample shown in Figure 2 was obtained after a heating and cooling cycle wherein the sample temperature was first increased from room temperature to 200 °C and then cooled to 0 °C. In an attempt to nucleate crystals in this sample, it was annealed at 0 °C for 24 h. In spite of this, the heating DSC scan of $pNte_{27}$ seen in Figure 2 contains no peaks. We also conducted DSC experiments on $pNte_{20}$ and $pNte_{10}$ and found no evidence of crystallinity.[34]

The DSC endotherms of all of the pNdc-*b*-pNte copolymers contain two peaks: one peak in the vicinity of 60 °C and another in the vicinity of 130 °C, as shown in Figure 2. The higher melting peak of $pNdc_{24}$-*b*-$pNte_{12}$, the copolymer with largest pNdc block, is very similar to that of pNdc homopolymers. We thus associate the higher melting peak with the melting of pNdc crystals in the block copolymers. We conclude that the lower melting peak must be associated with the melting of the pNte block. It is evident that the crystallization of the pNte block is entirely due to the formation of the lamellar microphase. The melting temperatures of the pNte crystals are similar to these reported for conventional poly(ethylene oxide) homopolymers.[40]

The key features of the DSC data obtained from both homopolypeptoids and block copolypeptoids are summarized in Figure 3. In Figure 3a, we plot the peak melting temperature of the pNdc crystals, $T_{m,Ndc}$, as a function of *n*, the number of Ndc monomers per chain. It is evident that the melting temperature of pNdc crystals in both homopolypeptoids and block copolypeptoids collapse on a single curve; $T_{m,Ndc}$ increases monotonically with *n*. Also shown in Figure 3a is the peak melting temperature of pNte crystals $T_{m,Nte}$, as a function of *n*. The general characteristics of the dependence of $T_{m,Nte}$ on *n* are similar to that of $T_{m,Ndc}$ on *n*. Note that a melting temperature of pNte crystals is governed by the length of the pNdc chains. In Figure 3b, we plot the specific enthalpy of melting of the pNte and pNdc crystals, $\Delta H_{m,Nte}$ and $\Delta H_{m,Ndc}$, as a function of *n*. The units of delta $H_{m,i}$ are J/g of i where *i* = Nte or Ndc. For $n \geq 12$, ΔH_{Ndc} is about 22 J/g for both homopolypeptoids and block copolypeptoids. Substantially lower values of $\Delta H_{m,Ndc}$ are obtained when $n < 12$. It is perhaps not surprising that $\Delta H_{m,Ndc}$ is governed by the length of pNdc chains or blocks. The value of $\Delta H_{m,Nte}$ of $pNdc_{24}$-*b*-$pNte_{12}$ is around 27 J/g, which is larger than $\Delta H_{m,Ndc}$ of the

dx.doi.org/10.1021/ja412123y | J. Am. Chem. Soc. 2014, 136, 2070−2077

same copolymer. It is perhaps interesting that the enthalpy required to melt the pNte crystals is higher than that of the pNdc crystals. In other words, the enthapy needed to melt the crystals induced in pNte is larger than that needed to melt the pNdc crystals that were responsible for their formation. At this point, we cannot offer any explanation for this surprising result. $\Delta H_{m,Ndc}$ is a monotonical function of n and it decreases rapidly to a value of 5 J/g for $n = 9$.

It is thus clear that our block copolymer samples have two kinds of lamellar phases: from room temperature to $T_{m,Nte}$ both pNdc and pNte lamellae are crystalline, while from $T_{m,Nte}$ to $T_{m,Ndc}$ only the pNdc lamellae are crystalline. In all cases, $T_{m,Ndc}$ determined by DSC is within experimental error of the transition temperature from the metastable state to disorder determined by SAXS.

The crystal structures adopted by pNte and pNdc chains were determined by wide-angle X-ray scattering (WAXS). Selected WAXS profiles obtained from our samples are shown in Figure 4. The room temperature WAXS profiles are

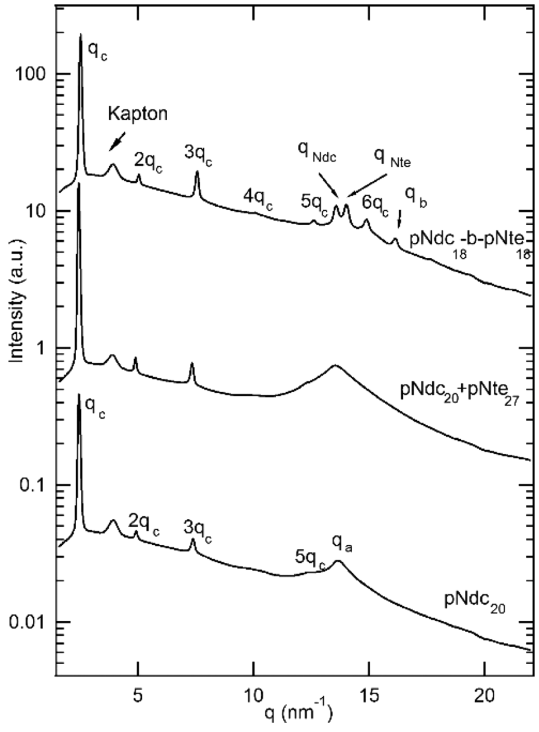

Figure 4. WAXS profiles at room temperature for pNdc$_{20}$, the blend of pNdc$_{20}$ and pNte$_{27}$, and diblock copolypeptoids pNdc$_{18}$-b-pNte$_{18}$ with different chain lengths. Profiles are vertically offset for clarity.

consistent with the proposed crystal structures presented in Figure 5. WAXS data from pNdc$_{20}$ homopolypeptoid (Figure 4) contains peaks at q_c, $2q_c$, $3q_c$, and $5q_c$, which reflect the spacing between the peptoid backbones parallel to the side chains, c ($c = 2\pi/q_c$), and an additional broad peak at $q = q_a$ which reflects the spacing between the peptoid backbones perpendicular to the side chains a ($a = 2\pi/q_a$). We note in passing that the WAXS q_c peak is also seen in the SAXS data at $q = 2.5$ nm^{-1}. Also shown in Figure 4 is the WAXS pattern obtained from a binary mixture of pNdc$_{20}$ and pNte$_{27}$ homopolymers at a molar ratio of 1:1. The WAXS profile of the mixture is identical to that of pNdc$_{20}$ homopolypeptoid. It is clear that blending pNdc with pNte does not induce crystallization of pNte chains. The WAXS profile of pNdc$_{18}$-*b*-

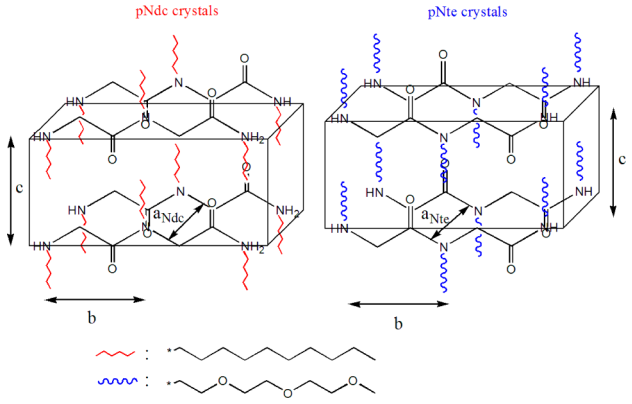

Figure 5. Two crystal structures of pNdc and pNte, where a_{Ndc} is the interchain distance of the pNdc block, a_{Nte} is the interchain distance of pNte block, b is distance between adjacent monomer residues, and c is the distance between peptoid chains.

pNte$_{18}$ has interesting features that are not seen in the homopolypeptoid. The broad peak at $q = q_a$ is replaced by a doublet, and an additional peak at $q = q_b$ is seen. We propose that the doublet reflects the value of a in the Ndc and Nte crystals. The values of a_{Ndc} and a_{Nte} thus obtained are 0.45 and 0.46 nm, respectively, while $b = 0.39$ nm. In addition, the higher order q_c peaks are better defined in pNdc$_{18}$-*b*-pNte$_{18}$ than those in pNdc$_{20}$. All of these characteristic lengths as determined by WAXS are mapped on to a proposed model, as indicated in Figure 5. It is clear that the pNte and pNdc crystals are very similar, likely due to their nearly isosteric side chains.

In order to study the effect of molecular volumes on the crystallization of pNte, we designed and synthesized the diblock copolymer poly-*N*-isoamylglycine-*block*-poly-*N*-2-(2-(2-methoxyethoxy)ethoxy)ethylglycine (pNia$_{18}$-*b*-pNte$_{18}$). pNia is a crystalline block but has a shorter alkyl side chain and a branch. In previous work, Rosales et al. demonstrated that the crystal structure of a pNia 15mer had a c of 1.5 nm, a of 0.46 nm, and b of 0.36 nm.[33] The dimensions of pNia crystals are close to those of pNdc, except for differences in c due to differences in side chain length. The DSC data from pNte$_{18}$-*b*-pNia$_{18}$ contain only one melting peak at 184 °C (Figure S1, Supporting Information), which is close to that of pNia homopolymers.[33] The missing pNte melting peak in pNia$_{18}$-*b*-pNte$_{18}$ confirms that isosteric monomers are essential for inducing crystallization of the pNte block. It is evident that this crystallization behavior can be controlled by tuning molecular structure.

The temperature dependence of the WAXS profiles was determined for pNdc$_{18}$-*b*-pNte$_{18}$ (Figure 6). Signatures of both pNte and pNdc crystals are seen up to 60 °C. At temperatures between 70 and 140 °C, only signatures of pNdc crystals are seen. All of the WAXS peaks disappear at 150 °C. In Figure 6b, we show the temperature dependence of the area under selected WAXS peaks at $q = q_{Nte}$ and $q = q_{Ndc}$. A discontinuous decrease in these areas is taken as a signature of melting of the crystals of pNte and pNdc, $T_{Wm,Nte}$ ($=T_{L''\text{-}L}$) and $T_{Wm,Ndc}$.

The phase transition temperatures determined from analysis of the SAXS data ($T_{L\text{-}M}$, $T_{M\text{-}D}$), the DSC data ($T_{m,Ndc}$ and $T_{m,Nte}$), and the WAXS data ($T_{Wm,Nte}$ and $T_{Wm,Ndc}$) are summarized in Table 2. It is clear that microphase separation in the pNdc-*b*-pNte copolymers is driven entirely by the crystallization of the pNdc blocks; note that $T_{m,Ndc}$ and $T_{Wm,Ndc}$ lie within the metastable window between the lamellar

dx.doi.org/10.1021/ja412123y | J. Am. Chem. Soc. 2014, 136, 2070−2077

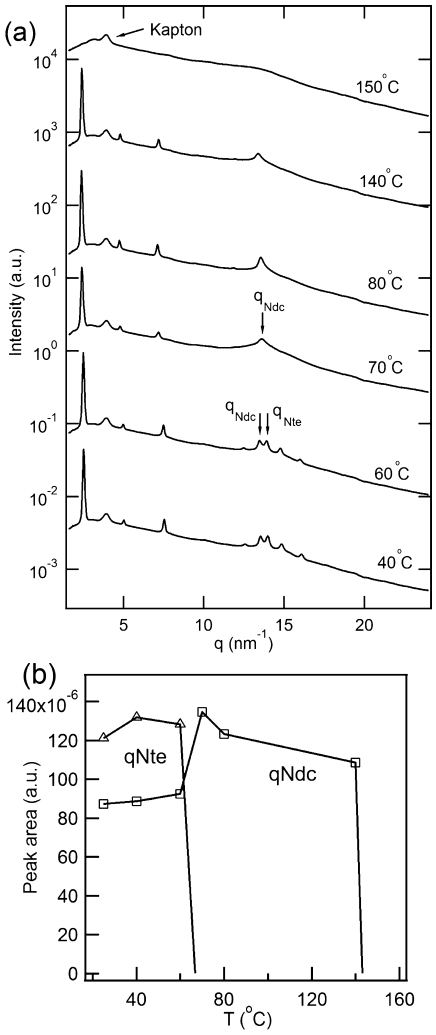

Figure 6. (a) WAXS intensity versus scattering vector, q, for $pNdc_{18}$-*b*-$pNte_{18}$ at selected temperatures. Profiles are vertically offset for clarity. (b) Open triangles plot the integration of the peak (q_{Nte}) of the WAXS profiles versus temperature, and open squares plot the integration of the peak (q_{Ndc}) of the WAXS profiles versus temperature.

microphase and disorder, as determined by SAXS. The melting temperatures of the pNte crystals determined by DSC and WAXS are in good agreement.

The characteristic length scale determined by SAXS and WAXS, d, c, a_{Nte}, a_{Ndc}, and b, are summarized in Table 3. The fully stretched end-to-end length of the block copolypeptoids (R) can be determined from the values of b, m, and n: $R = b(m + n)$ + end group contributions. Values of d/R for block copolypeptoid range from 0.75 to 0.81; see Table 3. Following Rosales et al.,[33] we suggest that the crystalline backbone of pNdc-*b*-pNte chains maybe tilted relative to the lamellar normal. Note that the signatures of "chain-folded lamellae" found in high molecular weight polymers synthesized by conventional polymerization techniques are absent in these polypeptoids.

Zhang et al. studied melting of high molecular weight linear and cyclic poly-*N*-decylglycine with values of n ranging from 40 to 300, synthesized by conventional solution polymerization.[35,41] They observed two melting peaks, which were attributed to the crystallization of the decyl side chain and the polypeptoid main chain. In our case, two melting peaks were only observed in the diblock copolymers; pNdc homopolymers with n ranging from 10 to 20 exhibited a single melting peak. The WAXS data reported by Zhang et al. are similar to those of pNdc homopolymers reported here; i.e., the two peaks at q_{Nte} and q_{Ndc} seen in our samples with two melting peaks were not observed by Zhang. We attribute the difference between data presented here and that reported by Zhang et al. to differences in chain length.

We obtained AFM images of $pNdc_{18}$-*b*-$pNte_{18}$, as shown in Figure 7a. These images suggest the presence of lamellar

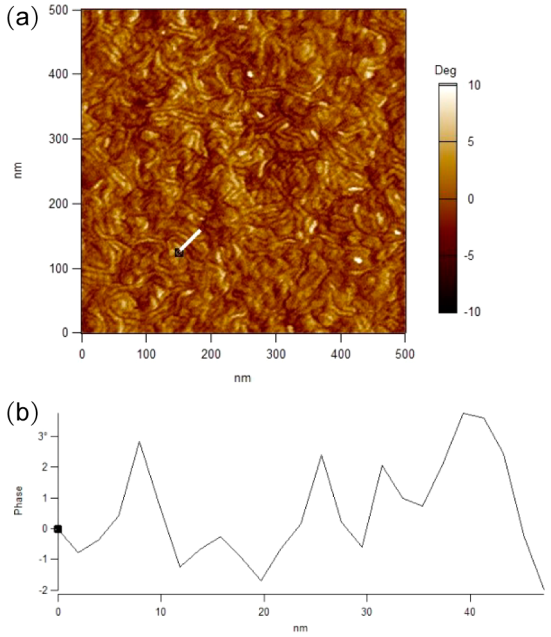

Figure 7. (a) AFM image of $pNdc_{18}$-*b*-$pNte_{18}$, casting from 10% $CHCl_3$ solution. (b) Height profile along the line indicated in part a.

morphology. Figure 7b shows the height profile along the line specified in Figure 7a. The average distance between the peaks in Figure 7b is 8.3 ± 1.4 nm, which is similar but smaller than the d spacing determined by SAXS, 10.8 nm. Our attempts to study the morphology of pNdc-*b*-pNte copolymers by transmission electron microscopy were not successful. Polarized optical microscopy was used to study one of our samples ($pNdc_{12}$-*b*-$pNte_{21}$). Birefringent patterns with line defects were

Table 3. Characteristics of the Block Copolypeptoids pNdc-*b*-pNte Obtained by SAXS (d) and WAXS[a]

polymers	ϕ_{Nte}	d (nm)	c (nm)	a_{Ndc} (nm)	a_{Nte} (nm)	b (nm)	R (nm)	d/R
$pNdc_9$-*b*-$pNte_{27}$	0.71	10.4	2.5	0.47	0.45	0.38	13.9	0.75
$pNdc_{12}$-*b*-$pNte_{21}$	0.59	9.9	2.5	0.46	0.45	0.39	13.1	0.76
$pNdc_{18}$-*b*-$pNte_{18}$	0.45	10.8	2.5	0.46	0.45	0.39	14.3	0.76
$pNdc_{24}$-*b*-$pNte_{12}$	0.29	11.3	2.5	0.46	0.45	0.38	13.9	0.81

[a] d is obtained by SAXS, and c, a_{Ndc}, a_{Nte}, and b are achieved by WAXS. R is the fully stretched end-to-end length of the block copolypeptoid.

dx.doi.org/10.1021/ja412123y | J. Am. Chem. Soc. 2014, 136, 2070−2077

observed below the final melting temperature of pNdc crystals, as shown in Figure S2 (Supporting Information). The crystal melts to give an isotropic phase at 145 °C. The polarized microscopy images in Figure 8 are consistent with the SAXS,

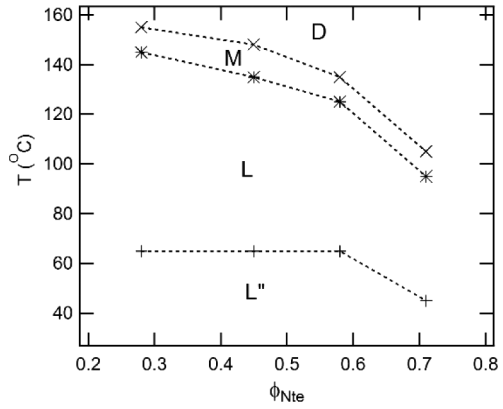

Figure 8. Phase diagram of pNdc-*b*-pNte at various temperature and volume fraction of pNte (ϕ_{Nte}), where D implies the disordered phase, M implies the metastable phase, L″ implies the lamellar phase with two crystalline blocks, and L implies the lamellar phase with crystalline pNdc block. The X's represent the transition between D and M (SAXS), the stars represent the transition between M and L (SAXS), the pluses represent the transition between L and L″ (WAXS), and the dotted lines are the estimated locations of phase boundaries.

WAXS, and DSC data presented above. Signatures of sphreulites that are often found in crystalline polymers are not seen in our samples in polarized microscopy images (and SAXS data presented in Figure 1).

The phase behavior of pNdc-*b*-pNte is summarized from the phase diagram in Figure 8, where the boundaries of the disordered phase (D), metastable window (M), the lamellar phase with the amorphous pNte and crystalline pNdc lamellae (L), and the lamellar phase with crystalline pNdc lamellae and induced pNdc crystals (L″) are shown as a function of composition. To our knowledge, the L″ phase is not reported previously.

CONCLUSION

A series of crystalline diblock copolypeptoids with polydispersity indices of 1.00017 or less was synthesized by solid-phase synthesis. The diblock copolymers comprised a poly-*N*-2-(2-(2-methoxyethoxy)ethoxy)ethylglycine (pNte) block and a poly-*N*-decylglycine (pNdc) block. pNte homopolymers are amorphous, while pNdc homopolymers are crystalline. The pNdc-*b*-pNte block copolymers self-assemble into a lamellar microphase. The formation of microphases is due entirely to the crystallization of the pNdc and not due to the Flory–Huggins interaction parameter between pNte and pNdc (χ). The lamellar to disorder transition temperature of the block copolymers is coincident with the melting of pNdc crystals. This observation is similar to that of Rangarajan et al.[17] The most surprising conclusion of our study is the formation of two crystalline lamellae (the L″ phase) at low temperatures. The crystallization of pNdc chains induces crystallization of pNte chains. The crystal structures of pNdc and pNte are very similar due, perhaps, to the nearly identical molecular volumes of the side chains. It is reasonable to believe that the crystallization of pNte induced by microphase separation is due to this similarity. We have thus demonstrated the highly tunable nature of the crystallization of pNte in diblock copolypeptoids. The melting of both pNdc and pNte crystals in our copolymers is governed by the chain length of the pNdc block. The fact that crystallization in one of the microphases in block copolymer is governed by the chain length of the other block is, perhaps, the most interesting consequence of the induced crystallization phenomenon that is reported here. We hope that this study will enhance our understanding of block copolymer crystallization and facilitate the discovery of highly functional polymer materials.

ASSOCIATED CONTENT

Supporting Information

The Experimental Section, DSC of block copolypeptoid $pNia_{18}$-*b*-$pNte_{18}$, and polarized optical microscopy for $pNdc_{12}$-*b*-$pNte_{21}$ and symbol definitions. This material is available free of charge via the Internet at http://pubs.acs.org.

AUTHOR INFORMATION

Corresponding Author

nbalsara@berkeley.edu; rnzuckermann@lbl.gov.

Author Contributions

All authors have given approval to the final version of the manuscript.

Notes

The authors declare no competing financial interest.

ACKNOWLEDGMENTS

Funding for this work was provided by the Soft Matter Electron Microscopy Program, supported by the Office of Science, Office of Basic Energy Science, U.S. Department of Energy, under Contract No. DE-AC02-05CH11231. The work was carried out at the Molecular Foundry and the Advanced Light Source at Lawrence Berkeley National Laboratory, both of which are supported by the Office of Science, Office of Basic Energy Science, U.S. Department of Energy, under Contract No. DE-AC02-05CH11231. Portions of this research were carried out at the Stanford Synchrotron Radiation Lightsource, a Directorate of SLAC National Accelerator Laboratory and an Office of Science User Facility operated for the U.S. Department of Energy Office of Science by Stanford University. We thank Dr. Adrianne M. Rosales for helpful advice and Dr. Gloria Olivier for help with XRD on the project.

REFERENCES

(1) Keller, A. *Rep. Prog. Phys.* **1968**, *31*, 623.
(2) McPherson, A. *Eur. J. Biochem.* **1991**, *1990*, 49–71.
(3) Massa, M. V.; Dalnoki-Veress, K. *Phys. Rev. Lett.* **2004**, *92*, 255509–255513.
(4) Kavassalis, T. A.; Sundararajan, P. R. *Macromolecules* **1993**, *26*, 4144–4150.
(5) Pearce, R.; Vancso, G. J. *Macromolecules* **1997**, *30*, 5843–5848.
(6) Hoffman, J. D. *Polym. Eng. Sci.* **1964**, *4*, 315–362.
(7) Stein, G. E.; Kramer, E. J.; Li, X.; Wang, J. *Phys. Rev. Lett.* **2007**, *98*, 086101.
(8) Zhu, L.; Cheng, S. Z. D.; Calhoun, B. H.; Ge, Q.; Quirk, R. P.; Thomas, E. L.; Hsiao, B. S.; Yeh, F.; Lotz, B. *J. Am. Chem. Soc.* **2000**, *122*, 5957–5967.
(9) Loo, Y.-L.; Register, R. A.; Ryan, A. J. *Phys. Rev. Lett.* **2000**, *84*, 4120–4123.
(10) Quiram, D. J.; Richard, A.; Marchand, G. R. *Macromolecules* **1997**, *30*, 4551–4558.
(11) Rangarajan, P.; Register, R. A.; Fetters, L. J.; Bras, W.; Naylor, S.; Ryan, A. J. *Macromolecules* **1995**, *28*, 4932–4938.

(12) Lee, L.-B. W.; Register, R. A. *Macromolecules* **2004**, *37*, 7278−7284.
(13) Ryan, A. J.; Hamley, I. W.; Bras, W.; Bates, F. S. *Macromolecules* **1995**, *28*, 3860−3868.
(14) Hamley, I. *Adv. Polym. Sci.* **1999**, *148*, 113−137.
(15) Deplace, F.; Scholz, A. K.; Fredrickson, G. H.; Kramer, E. J.; Shin, Y.-W.; Shimizu, F.; Zuo, F.; Rong, L.; Hsiao, B. S.; Coates, G. W. *Macromolecules* **2012**, *45*, 5604−5618.
(16) Liu, X.-B.; Zhao, Y.-F.; Chen, E.-Q.; Ye, C.; Shen, Z.-H.; Fan, X.-H.; Cheng, S. Z. D.; Zhou, Q.-F. *Macromolecules* **2008**, *41*, 5223−5229.
(17) Rangarajan, P.; Register, R. A.; Fetters, L. J. *Macromolecules* **1993**, *26*, 4640−4645.
(18) Loo, Y.-L.; Register, R. A.; Ryan, A. J. *Macromolecules* **2002**, *35*, 2365−2374.
(19) Loo, Y.-L.; Richard, A.; Ryan, A. J.; Dee, G. T. *Macromolecules* **2001**, *34*, 8968−8977.
(20) Mai, S. M.; Fairclough, J. P. A.; Viras, K.; Gorry, P. A.; Hamley, I. W.; Ryan, A. J.; Booth, C. *Macromolecules* **1997**, *30*, 8392−8400.
(21) Yang, J.; Liang, Y.; Luo, J.; Zhao, C.; Han, C. C. *Macromolecules* **2012**, *45*, 4254−4261.
(22) Lin, M.-C.; Chen, H.-L.; Su, W.-B.; Su, C.-J.; Jeng, U. S.; Tzeng, F.-Y.; Wu, J.-Y.; Tsai, J.-C.; Hashimoto, T. *Macromolecules* **2012**, *45*, 5114−5127.
(23) Ding, Y.; Rabolt, J. F.; Chen, Y.; Olson, K. L.; Baker, G. L. *Macromolecules* **2002**, *35*, 3914−3920.
(24) Li, Y.; Ma, Y.; Li, J.; Jiang, X.; Hu, W. *J. Chem. Phys.* **2012**, *136*, 104906.
(25) Rosales, A. M.; Segalman, R. A.; Zuckermann, R. N. *Soft Matter* **2013**, *9*, 8400−8414.
(26) Sun, J.; Zuckermann, R. N. *ACS Nano* **2013**, *7*, 4715−4732.
(27) Simon, R. J.; Kania, R. S.; Zuckermann, R. N.; Huebner, V. D.; Jewell, D. A.; Banville, S.; Ng, S.; Wang, L.; Rosenberg, S.; Marlowe, C. K. *Proc. Natl. Acad. Sci. U. S. A.* **1992**, *89*, 9367−9371.
(28) Zuckermann, R. N.; Kodadek, T. *Curr. Opin. Mol. Ther.* **2009**, *11*, 299−307.
(29) Zhang, D.; Lahasky, S. H.; Guo, L.; Lee, C.-U.; Lavan, M. *Macromolecules* **2012**, *45*, 5833−5841.
(30) Luxenhofer, R.; Fetsch, C.; Grossmann, A. *J. Polym. Sci., Part A: Polym. Chem.* **2013**, *51*, 2731−2752.
(31) Zuckermann, R. N.; Kerr, J. M.; Kent, S. B. H.; Moos, W. H. *J. Am. Chem. Soc.* **1992**, *114*, 10646−10647.
(32) Tran, H.; Gael, S. L.; Connolly, M. D.; Zuckermann, R. N. *JoVE* **2011**, e3373.
(33) Rosales, A. M.; Murnen, H. K.; Zuckermann, R. N.; Segalman, R. A. *Macromolecules* **2010**, *43*, 5627−5636.
(34) Sun, J.; Stone, G. M.; Balsara, N. P.; Zuckermann, R. N. *Macromolecules* **2012**, *45*, 5151−5156.
(35) Lee, C.-U.; Smart, T. P.; Guo, L.; Epps Iii, T. H.; Zhang, D. *Macromolecules* **2011**, *44*, 9574−9585.
(36) Sun, J.; Liao, X.; Teran, A.; Balsara, N. P.; Zuckermann, R. N. *J. Am. Chem. Soc.* **2013**, *135*, 14119−14124.
(37) Leibler, L. *Macromolecules* **1980**, *13*, 1602−1617.
(38) Khandpur, A. K.; Foerster, S.; Bates, F. S.; Hamley, I. W.; Ryan, A. J.; Bras, W.; Almdal, K.; Mortensen, K. *Macromolecules* **1995**, *28*, 8796−8806.
(39) Lodge, T. P.; Blazey, M. A.; Liu, Z.; Hamley, I. W. *Macromol. Chem. Phys.* **1997**, *198*, 983−995.
(40) Money, B. K.; Swenson, J. *Macromolecules* **2013**, *46*, 6949−6954.
(41) Lee, C.-U.; Ang, L.; Kushal, G.; Zhang, D. *Macromolecules* **2013**, *46*, 8213−8223.